Reconstruction of $ZH \to q\bar{q}W^+W^-$ and $ZH \to \ell^+\ell^-W^+W^-$ Final States with Linear e^+e^- Collider

A. Raspereza
DESY, Platanenallee 6, D-15738 Zeuthen, Germany

The potential of a e^+e^- linear collider operated at a centre-of-mass energy of about 350 GeV for the reconstruction of the $ZH \to q\bar{q}W^+W^-$ and $ZH \to \ell^+\ell^-W^+W^-$ final states is studied. Higgs masses of 120, 150 and 180 GeV are considered.

1 Introduction

An e^+e^- collider with centre–of–mass energy $\sqrt{s}$ of a few hundred GeV is particularly well suited to discover the Higgs boson if its mass is of $\mathcal{O}(100\text{ GeV})$. Even in the case a particle interpreted as the Higgs boson was discovered already at another accelerator like LHC a linear collider would provide an optimal scenario for identifying it as the Higgs boson predicted by the Standard Model [1]. Crucial tests here are the values of the couplings to gauge bosons and fermions. A quantity which depends on the couplings to the gauge bosons is the Higgs boson production cross section in the Higgs-strahlung or fusion process. The couplings to different fermion species and gauge bosons are accessible by the measurement of the Higgs boson branching fractions.

In this letter, the author describes a procedure of the reconstruction of the $ZH \to q\bar{q}W^+W^-$ and $ZH \to \ell^+\ell^-W^+W^-$ ($\ell = e, \mu$) final states with subsequent decay of W-bosons into a pair of quarks. Along with simultaneous determination of the inclusive cross section in the Higgs-strahlung process [2] this method allows the measurement of the branching fraction of the Higgs boson into pair of W-bosons. Moreover, the present analysis is also used to measure the mass of the Higgs boson.

The analysis takes into account the detector resolutions, the efficiencies of lepton identification and the relevant background processes.

2 Experimental Conditions

The study is performed for a linear collider operated at a centre–of–mass energy of 350 GeV. The assumed data statistics corresponds to an integrated luminosity of 500 fb^{-1}. The detector used in the simulation follows the proposal presented in the TESLA Conceptual Design Report [3].

The interaction region is surrounded by a central tracker consisting of a silicon microvertex detector as the innermost part and a time projection chamber. In the radial direction follows an electromagnetic calorimeter, a hadron calorimeter, the coils of a superconducting magnet and an instrumented iron flux return yoke. The solenoidal magnetic field is 3 Tesla. The central tracker momentum resolution is

$$\sigma_{\mathrm{p_t}}/\mathrm{p_t} = 7 \cdot 10^{-5} \cdot \mathrm{p_t} \ (\mathrm{GeV}).$$

The energy resolutions of the electromagnetic and hadronic calorimeters are

$$\frac{\sigma_{\mathrm{E_{ecal}}}}{\mathrm{E_{ecal}}} = \frac{10\%}{\sqrt{\mathrm{E_{ecal}}}} + 0.6\%, \quad \frac{\sigma_{\mathrm{E_{hcal}}}}{\mathrm{E_{hcal}}} = \frac{50\%}{\sqrt{\mathrm{E_{hcal}}}} + 4\%, \ \ \mathrm{E}\ (\mathrm{GeV}).$$

The polar angular coverage of the central tracker maintaining the resolution is $|\cos\theta| < 0.85$, above this range the tracking resolution degrades. The electromagnetic and hadron calorimeters cover the region $|\cos\theta| < 0.996$, maintaining the resolution over the whole angular range. The simulation of the detector is done with the program SIMDET [4].

3 Analysis

3.1 Signal and Background

Events of the signal, $\mathrm{e^+e^-} \to \mathrm{ZH}$, are generated using the PYTHIA program [5] for Higgs boson masses of 120, 150 and 180 GeV. The Standard Model cross sections and the expected event numbers corresponding to a luminosity of 500 $\mathrm{fb^{-1}}$ are given in Table 1.

Process	$\mathrm{M_H}$ (GeV)	σ (fb)	events
$\mathrm{e^+e^-} \to \mathrm{ZH} \to \ell^+\ell^-\mathrm{W^+W^-}$	120	0.58	2.9×10^2
$\ell = \mathrm{e}, \mu$	150	2.6	1.3×10^3
$\mathrm{W^\pm} \to \mathrm{q\bar{q}'}$	180	2.6	1.3×10^3
$\mathrm{e^+e^-} \to \mathrm{ZH} \to \mathrm{q\bar{q}W^+W^-}$	120	6.0	3.0×10^3
$\ell = \mathrm{e}, \mu$	150	26.5	1.3×10^4
$\mathrm{W^\pm} \to \mathrm{q\bar{q}'}$	180	26.6	1.3×10^4

Table 1: The signal cross sections for different Higgs boson masses and the number of expected events for a luminosity of 500 $\mathrm{fb^{-1}}$.

For the background studies the following Monte Carlo generators are used: PYTHIA for $\mathrm{e^+e^-} \to \mathrm{e^+e^-f\bar{f}}$, $\mathrm{e^+e^-} \to (\mathrm{Z}/\gamma) \to \mathrm{f\bar{f}}(\gamma)$, $\mathrm{e^+e^-} \to \mathrm{W^+W^-}$ and $\mathrm{e^+e^-} \to \mathrm{ZZ}$, and EXCALIBUR [6] for non-resonant $\mathrm{Ze^+e^-}$ and $\mathrm{Z}\nu_\mathrm{e}\bar{\nu}_\mathrm{e}$ and for

background process	events
$e^+e^- \to e^+e^- f\,f$	2.0×10^9
$e^+e^- \to f\,\bar{f}(\gamma)$	2.0×10^7
$e^+e^- \to W^+W^-$	7.0×10^6
$e^+e^- \to ZZ$	5.0×10^5

Table 2: The number of events expected for several background sources.

$We\nu_e$. The number of events expected in the most important background processes is given in Table 2.

Initial state bremsstrahlung is simulated with PYTHIA. Beamstrahlung is taken into account using the CIRCE program [7].

Both signal and background events are processed by the detector simulation package SIMDET. The output in terms of reconstructed track momenta and calorimetric cluster energies is used for the forthcoming analysis.

3.2 Kinematic Fit

The method described in this letter is based on exclusive measurement of $ZH \to q\bar{q}W^+W^-$ or $ZH \to \ell^+\ell^-W^+W^-$ final states. Therefore a kinematic fit imposing energy-momentum conservation can be performed to improve the mass resolution. Angular and energy resolutions are used as inputs in the routine performing the kinematic fit. They are different for isolated leptons and jets. The resolution functions obtained from Monte-Carlo studies are presented in Table 3.

Measured object	$\frac{\sigma_E}{E}$	σ_Θ	σ_ϕ
Lepton	$10^{-4} \cdot E$ [GeV]	1 mrad	$\frac{1\ \text{mrad}}{\sin\Theta}$
Jet	$\frac{20\%}{\sqrt{E\ [\text{GeV}]}}$	10 mrad	$\frac{10\ \text{mrad}}{\sin\Theta}$

Table 3: Energy and angular resolutions used in kinematic fit.

The kinematic fit is performed using package [8].

3.3 $ZH \to \ell^+\ell^-W^+W^-$ Analysis

We consider W-boson decays into two quarks, hence the topology of this final state is two leptons and four jets. Electrons are identified as energy depositions in the electromagnetic calorimeter whose shape is compatible with the expectation for an electromagnetic shower and with a matched track in the central tracker. The measured track momentum and shower energy must be in agreement within 5% and the shower leakage into the hadron calorimeter must be less than 2 GeV. Muons are tracks pointing to energy depositions in the calorimeters which are consistent with the expectation for a minimum ionising particle. Both electrons and muons must have momenta larger than 10 GeV and fulfil the polar angle cut $|\cos\theta| < 0.9$. To suppress ZZ background the production polar angle of the two-lepton-system must be $|\cos\theta_{\mathrm{ll}}| < 0.6$.

Two different selections are applied depending on the mass of the Higgs boson, $\mathrm{M_H}$.

High mass selection ($\mathrm{M_H}$ = 150, 180 GeV)

An event is selected if it satisfies the following criteria:

- visible energy: $\mathrm{E_{vis}} > 300$ GeV;
- number of energy flow objects: $\mathrm{N_{EFO}} > 50$;
- at least two identified electrons or muons with opposite charges;
- polar angle of event thrust: $|\cos\Theta_{\mathrm{T}}| < 0.95$;
- event thrust: $\mathrm{T} < 0.9$;
- Fox-Wolfram moment of second order: $\mathrm{H_2} < 0.45$;
- invariant mass of di-lepton system has to be 10 GeV within Z mass.

With these requirements high multiplicity events with two identified leptons stemming from Z are selected. The signal selection efficiencies and the number of expected signal and background events are summarised in Table 4.

Tracks and calorimetric energy depositions not stemming from leptons are grouped into four jets using the Durham algorithm [9]. Then a 4C fit requiring energy-momentum conservation is applied to the system of two leptons and four jets. The mass of the Higgs boson is reconstructed as invariant mass of four-jet system. It should be noted that background events mainly concentrate in the vicinity of Z mass and only a small percentage (<5 %) of background events have a reconstructed mass of the hadronic system greater that 140 GeV.

Process	Selection efficiency	Expected events
ZH $\rightarrow \ell^+\ell^- W^+W^-$ (M_H=150 GeV)	63.9±2.2%	$8.4{\cdot}10^2$
ZH $\rightarrow \ell^+\ell^- W^+W^-$ (M_H=180 GeV)	71.7±2.3%	$9.5{\cdot}10^2$
$e^+e^- \rightarrow$ ZZ	-	$3.6{\cdot}10^3$
Other background sources	-	40

Table 4: The signal selection efficiencies and the number of expected signal and background events in the case of high mass ZH $\rightarrow \ell^+\ell^- W^+W^-$ selection. Reported numbers correspond to a luminosity of 500 fb^{-1} and are quoted for entire mass spectrum.

Low mass selection (M_H = 120 GeV)

First, the high mass selection is applied. To further suppress ZZ background a binned likelihood approach [10] is exploited. The final discriminant is calculated using the likelihood technique and considering two classes of processes: $e^+e^- \rightarrow$ ZZ and ZH $\rightarrow \ell^+\ell^- W^+W^-$. Four discriminating variables are combined into the likelihood:

- Fox-Wolfram moment of second order: H_2;
- number of energy flow objects: N_{EFO};
- jet resolution parameter for which the number of jets in the hadronic system changes from 4 to 3: Y_{34};
- jet resolution parameter for which the number of jets in the hadronic system changes from 3 to 2: Y_{23}.

The distributions of these variables for ZZ background and signal are presented in Figure 1. The final discriminant is shown in Figure 2.

Events are accepted into final sample if the value of the final discriminant is greater than 0.95. Moreover, good quality of the 4C kinematic fit is required by applying cut $\chi^2_{4C} < 10$. The signal selection efficiency and the number of expected background and signal events are given in Table 5.

Process	Selection efficiency	Expected events
ZH $\rightarrow \ell^+\ell^- W^+W^-$ (M_H=120 GeV)	25.0±2.9%	75
$e^+e^- \rightarrow$ ZZ	-	90
Other background sources	-	< 5

Table 5: The signal selection efficiency and the number of expected signal and background events in the case of low mass ZH $\rightarrow \ell^+\ell^- W^+W^-$ selection. Reported numbers correspond to a luminosity of 500 fb^{-1} and are quoted for entire mass spectrum.

Four-jet invariant mass distributions are shown in Figure 3.

3.4 $ZH \to q\bar{q}W^+W^-$ Analysis

Since we consider W-boson decays into two quarks, the signature of this final state is six jets. Selection of six-jet events proceeds in two steps. At first stage a loose preselection of hadronic events is applied. These events must pass the following criteria:

- visible energy: $\mathrm{E_{vis}} > 275$ GeV;
- event thrust: $\mathrm{T} < 0.9$;
- polar angle of event thrust: $|\cos\Theta_\mathrm{T}| < 0.95$;
- no isolated energetic leptons;
- jet resolution parameter: $\log \mathrm{Y}_{56} >$ -0.8.

The likelihood technique is applied at the next stage of the analysis. Four event classes are considered: $\mathrm{e^+e^-} \to \mathrm{ZZ}$, $\mathrm{e^+e^-} \to \mathrm{W^+W^-}$, $\mathrm{e^+e^-} \to \mathrm{q\,\bar{q}}(\gamma)$, $\mathrm{ZH} \to \mathrm{q\bar{q}W^+W^-}$. The final discriminant is the likelihood combined of the following six variables:

- Fox-Wolfram moment of second order: $\mathrm{H_2}$;
- number of energy flow objects: $\mathrm{N_{EFO}}$;
- event sphericity: S;
- event thrust: T;
- jet resolution parameter: Y_{34};
- jet resolution parameter: Y_{56}.

The distributions of these variables for different background processes and signal are shown in Figures 4 and 5. The distribution of the final discriminant for $\mathrm{M_H}$=150 GeV is shown in Figure 6.

Depending on $\mathrm{M_H}$, events are accepted into final sample when the value of the final discriminant is larger than given threshold. $\mathrm{M_H}$ is reconstructed as invariant mass of four-jet system assigned to W-bosons. The large number of four-jet combinations in six-jet events results in a large combinatorial background. This background can be essentially reduced by choosing only one combination that satisfies best the hypothesis of $\mathrm{ZH} \to \mathrm{q\bar{q}W^+W^-}$ production. In the case when $\mathrm{M_H} > 2\mathrm{M_W}$ both W-bosons are produced on mass shell while in the case when $\mathrm{M_H} < 2\mathrm{M_W}$ only one of W-bosons is produced on-shell. This feature is used to optimally combine six jets into three pairs. For M_H=120, 150 GeV only one W is expected to be on the mass shell. Therefore the quantity

$$\chi^2 = (M_{ij} - M_Z)^2/\sigma_Z^2 + (M_{kl} - M_W)^2/\sigma_W^2$$

is calculated for all possible di-jet combinations, where M_{ij} - invariant mass of two jets assigned to Z and M_{kl} - invariant mass of two jets assigned to W. Quantities σ_Z and σ_W are convolutions of bosonic widths and mass resolutions. They are estimated to be 4.1 GeV and 4.3 GeV respectively. For Higgs boson mass M_H=180 GeV both W-bosons are on-shell. Again all di-jet combinations are taken and quantity

$$\chi^2 = (M_{ij} - M_Z)^2/\sigma_Z^2 + (M_{kl} - M_W)^2/\sigma_W^2 + (M_{mn} - M_W)^2/\sigma_W^2$$

is calculated, where M_{mn} - the mass of the two jets stemming from the second W-boson. The jet pairing with the smallest χ^2 is chosen and subject of a 5C kinematic fit imposing energy-momentum conservation and constraining the mass of the two jets stemming from Z to M_Z. Good quality of 5C fit is required by applying cut $\chi^2_{5C} < 10$. The signal selection efficiencies and background composition of events accepted into final sample are given in Table 6.

$M_H =$	120 GeV	150 GeV	180 GeV
$e^+e^- \to ZZ$	70	$5.0{\cdot}10^2$	$3.4{\cdot}10^2$
$e^+e^- \to W^+W^-$	310	$3.8{\cdot}10^3$	$1.8{\cdot}10^3$
$e^+e^- \to q\,\bar{q}(\gamma)$	500	$6.2{\cdot}10^3$	$4.4{\cdot}10^3$
$ZH \to q\bar{q}W^+W^-$	130	$3.9{\cdot}10^3$	$2.7{\cdot}10^3$
Selection Efficiency	4.3±0.3 %	29.5±0.5 %	21.0±0.4 %

Table 6: The signal selection efficiencies and the number of expected signal and background events in the case of $ZH \to q\bar{q}W^+W^-$ analysis. Reported numbers correspond to a luminosity of 500 fb^{-1} and are quoted for entire mass spectrum.

The distributions of the invariant mass of four-jet system assigned to W-bosons are shown in Figure 7.

4 Results

The obtained mass spectra are fitted with a superposition of a signal and a background distribution. To account for asymmetric signal shape in the case of $ZH \to \ell^+\ell^-W^+W^-$ final state the left side of the signal is fitted with a Gaussian while the right side is parametrised as the sum of a Gaussian and exponential function. The signal mass spectra resulting from $ZH \to q\bar{q}W^+W^-$

final states are fitted with a Gaussian. The background shape is approximated by polynomial function of second order.

A binned χ^2 fit is performed with the mass, M_X, the width, σ_X, and normalisation of the signal as free parameters. The masses M_X agree well with the values used in the signal generation. The statistical uncertainty of the mass determination, the relative error of the cross-section measurement and the mass resolution are given in Table 7.

Process	M_H (GeV)	ΔM_H (MeV)	σ_{M_H} (GeV)	$\Delta\sigma/\sigma$ (%)
$ZH \to \ell^+\ell^- W^+W^-$	120	310	1.9	13.0
$\ell = e, \mu$	150	95	1.8	5.2
$W^\pm \to q\bar{q}'$	180	100	1.7	4.0
$ZH \to q\bar{q} W^+W^-$	120	250	2.0	12.0
$\ell = e, \mu$	150	100	2.9	4.6
$W^\pm \to q\bar{q}'$	180	110	3.1	4.4

Table 7: Accuracy of the mass determination, ΔM_H, mass resolution, σ_{M_H}, and relative error of the cross-section determination, $\Delta\sigma/\sigma$.

For the high masses of the Higgs boson (M_H=150, 180 GeV) the value of the uncertainty of the mass determination is about 100 MeV while the relative error of the cross-section measurement is between 4 and 5%. The accuracy of the mass and cross-section determination deteriorates at low mass of the Higgs boson (M_H=120 GeV) due to lower cross-section of relevant processes and tighter selection criteria. Both these factors result in lower signal statistics and larger errors of measurement at low Higgs boson masses.

5 Acknowledgements

I would like to express my gratitude to Wolfgang Lohmann and Pablo Garcia-Abia for fruitful discussions and support in preparation of this letter.

References

1. S.L. Glashow, *Nucl. Phys.* **22**, 579 (1961);
   S. Weinberg, *Phys. Rev. Lett.* **19**, 1264 (1967);
   A. Salam, "Weak and Electromagnetic Interactions", in *Elementary Particle Theory*, edited by N. Svartholm, page 367, Stockholm, 1969, Almqvist and Wiksell.
2. P. Garcia-Abia, W. Lohmann, *EPJdirect* **C2**, 1-6 (2000).
3. "Conceptual Design of a 500 GeV e^+e^- Linear Collider with Integrated X-ray Laser Facility", Vol. I, editors R. Brinkmann, G. Materlik, J. Rossbach, A. Wagner, DESY 1997-048, ECFA 1997-182.
4. SIMDET V3.1, M. Pohl and H.J. Schreiber, DESY-99-030 (1999).
5. PYTHIA V6.115, T. Sjöstrand, Comp. Phys. Comm. 82 (1994) 74.
6. R. Kleiss and R. Pittau, Comp. Phys. Comm. 85 (1995) 447;
   R. Pittau, Phys. Lett. B 335 (1994) 490.
7. T. Ohl, The CIRCE program (V6), IKDA 96/13-rev (1996), hep-ph/9607454-rev;
   H. Anlauf, IKDA 96/6 (1996), hep-ph/9602397.
8. http://www.desy.de/˜blobel.
9. S.Bethke *et al.*, *Nucl. Phys.* **B370**, 310 (1992).
10. OPAL Collaboration, K. Ackerstaff *et al.*, *Eur. Phys. J.* **C1**, 425 (1998).

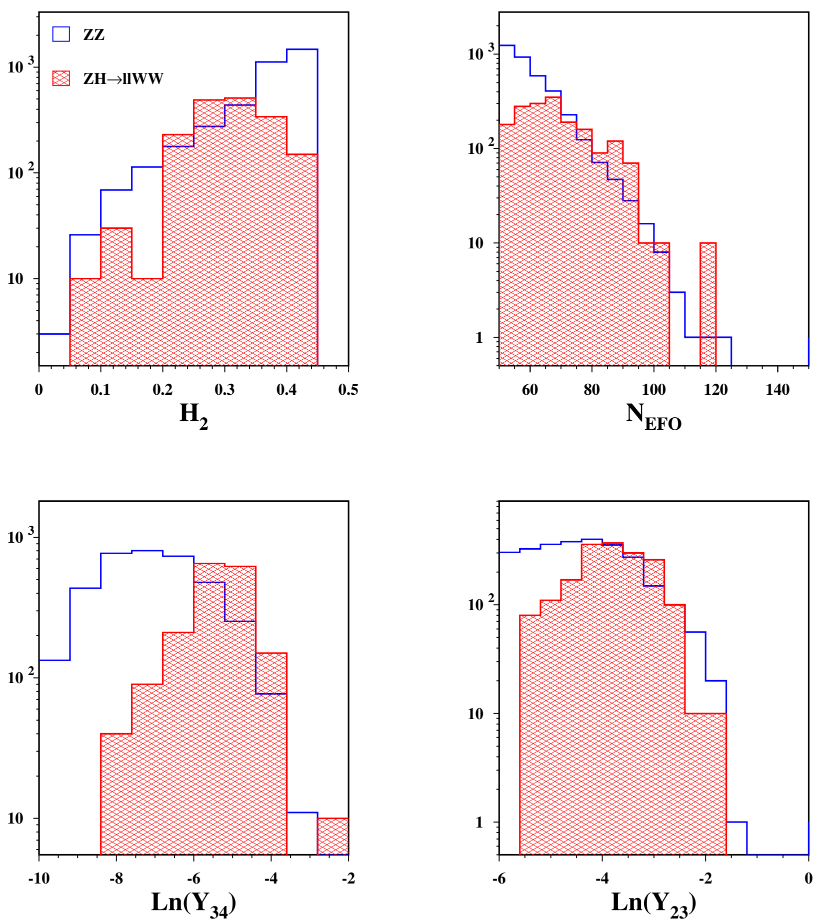

Figure 1: Distributions of variables used to combine the ZH $\rightarrow \ell^+\ell^-W^+W^-$ likelihood: Fox-Wolfram moment of second order (upper-left); number of energy flow objects (upper-right); logarithm of Y_{34} parameter (lower-left); logarithm of Y_{23} parameter (lower-right). Signal is scaled by factor 10.

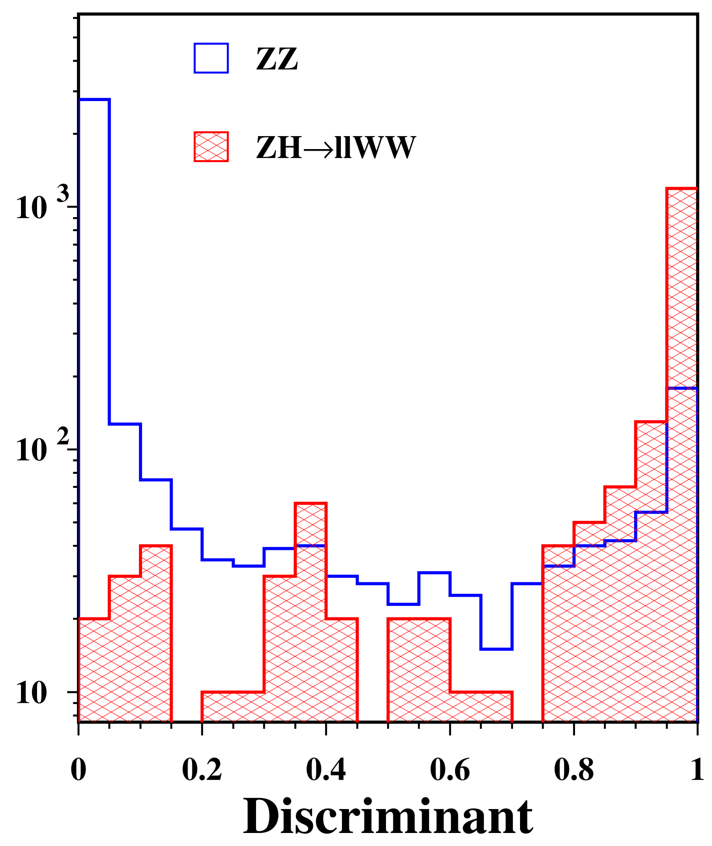

Figure 2: Final discriminant used in low mass ZH $\rightarrow \ell^+\ell^- W^+W^-$ selection. Signal is scaled by factor 10.

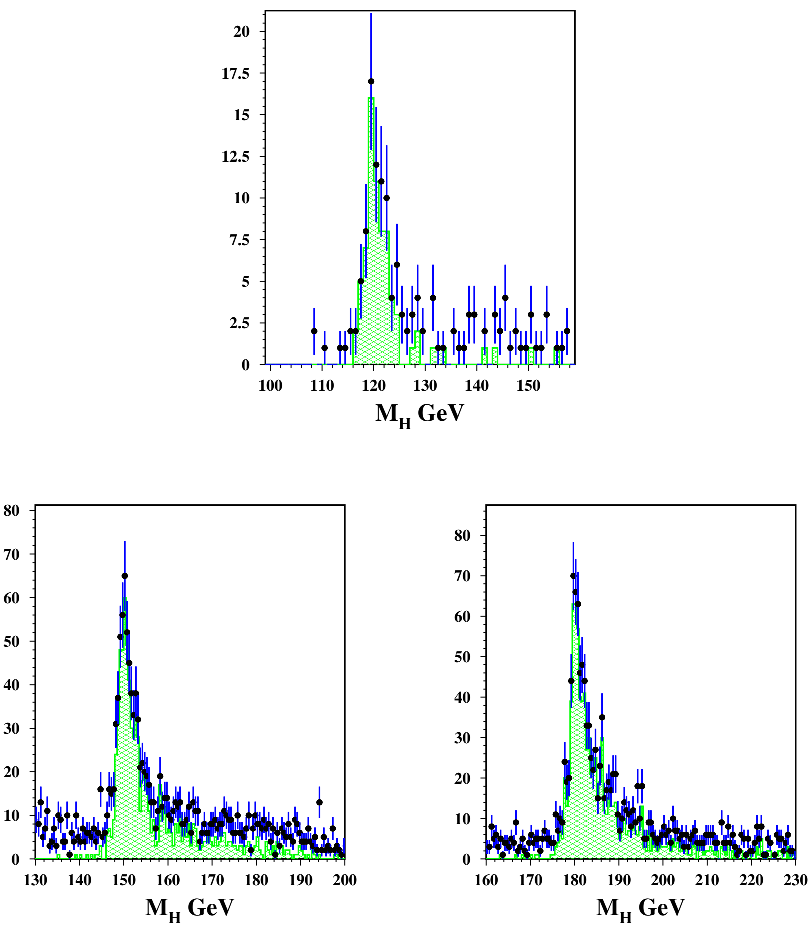

Figure 3: Mass spectra in ZH $\rightarrow$ $\ell^+\ell^-W^+W^-$ analysis: M_H=120 GeV (upper); M_H=150 GeV (lower-left); M_H=180 GeV (lower-right). Hatched histograms correspond to signal. Dots stand for to superposition of signal and background.

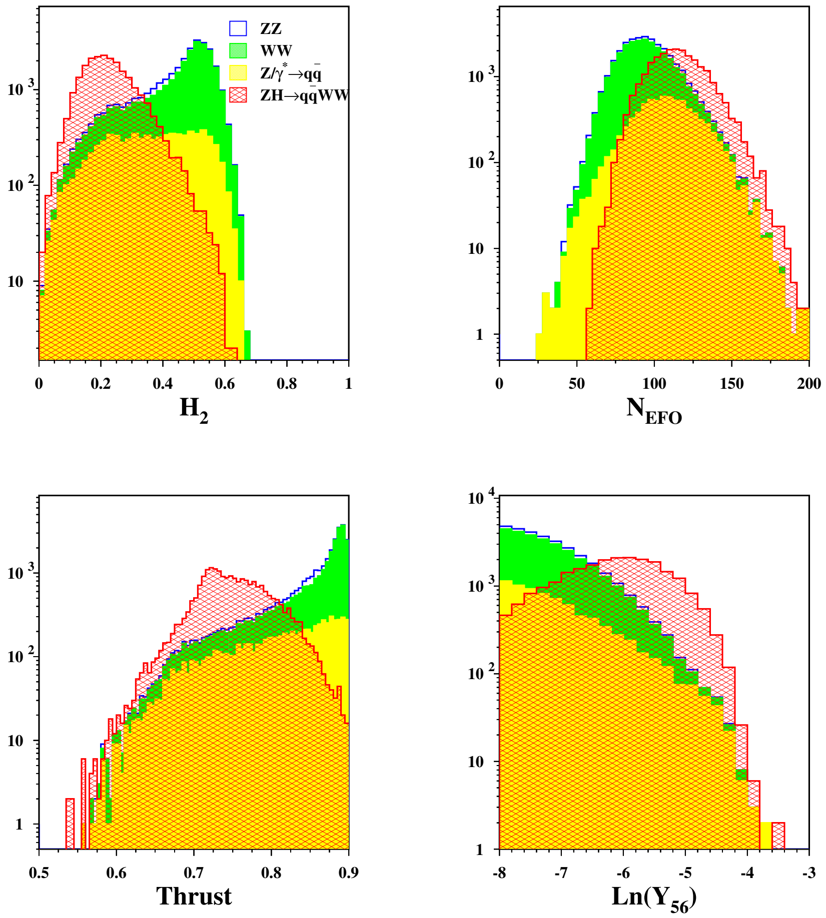

Figure 4: Distributions of variables used to combine the ZH $\rightarrow$ q$\bar{\text{q}}$W$^+$W$^-$ likelihood: Fox-Wolfram moment of second order (upper-left); number of energy flow objects (upper-right); event thrust (lower-left); logarithm of Y_{56} parameter (lower-right). Signal is scaled by factor 2. Background is scaled by factor 1/20. M_H=150 GeV.

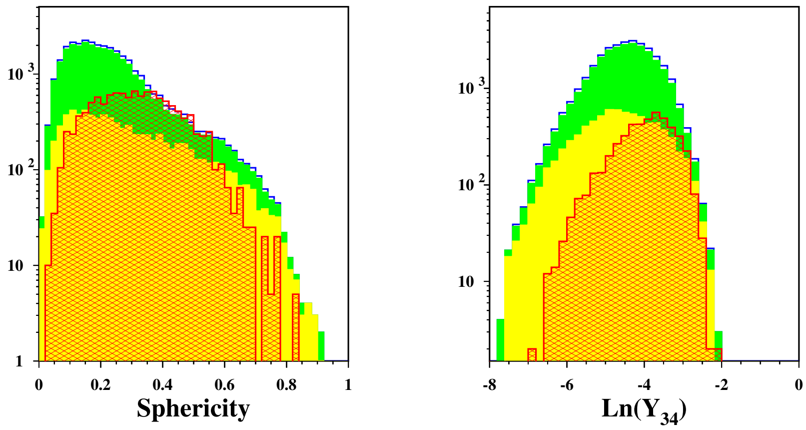

Figure 5: Distributions of variables used to combine the ZH $\rightarrow q\bar{q}W^+W^-$ likelihood: event sphericity(left); logarithm of Y_{34} parameter (right). Signal is scaled by factor 2. Background is scaled by factor 1/20. M_H=150 GeV.

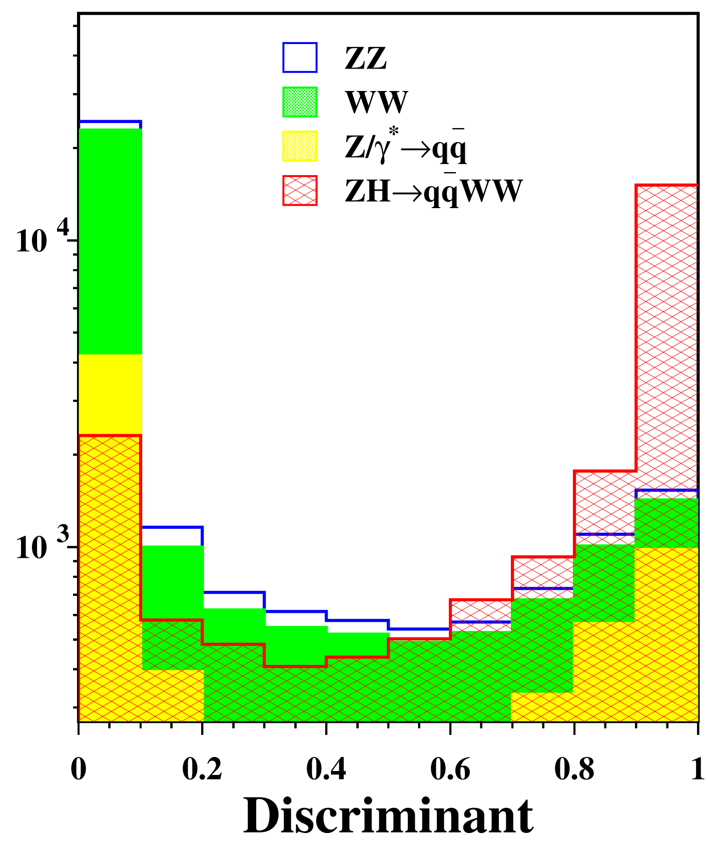

Figure 6: Final discriminant used in ZH $\rightarrow$ q$\bar{\mathrm{q}}$W$^+$W$^-$ selection. Signal is scaled by factor 5. Background is scaled by factor 1/20. The mass of the Higgs boson M_H=150 GeV.

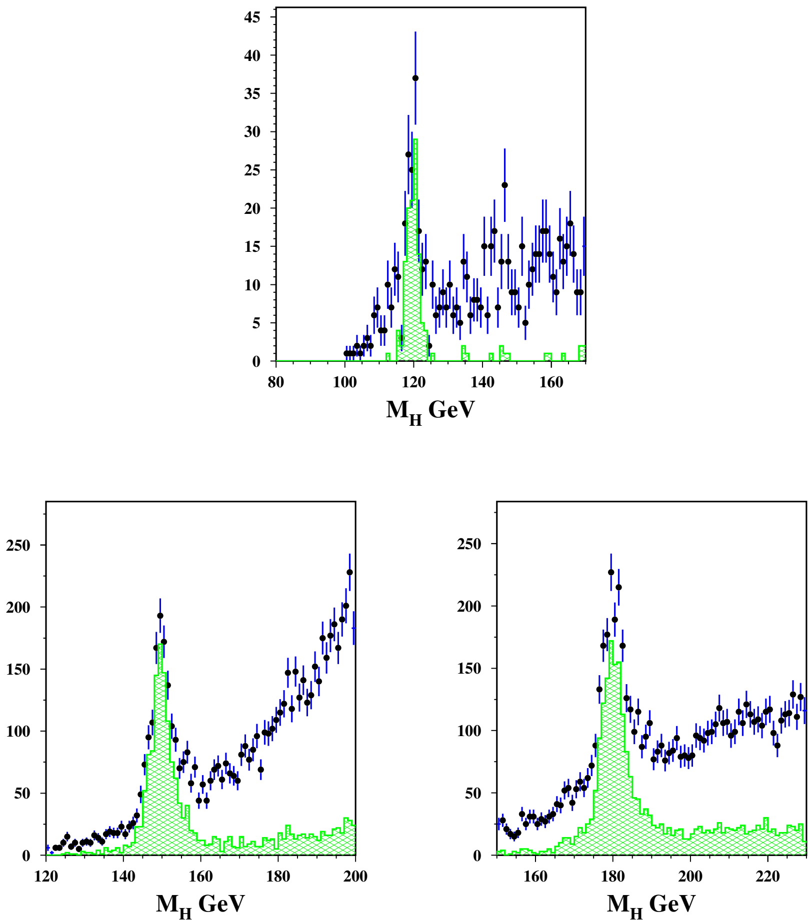

Figure 7: Mass spectra in ZH $\rightarrow$ $q\bar{q}W^+W^-$ analysis: M_H=120 GeV (upper); M_H=150 GeV (lower-left); M_H=180 GeV (lower-right). Hatched histograms correspond to signal. Dots stand for superposition of signal and background.